Author/s:
Martin-Sanchez, C;Antonio Barreda-Argueso, J;Seibt, S;Mulvaney, P;Rodriguez, F

Title:
Effects of Hydrostatic Pressure on the Surface Plasmon Resonance of Gold Nanocrystals

Date:
2019-01

Citation:
Martin-Sanchez, C., Antonio Barreda-Argueso, J., Seibt, S., Mulvaney, P. & Rodriguez, F. (2019). Effects of Hydrostatic Pressure on the Surface Plasmon Resonance of Gold Nanocrystals. ACS Nano, 13 (1), pp.498-504. https://doi.org/10.1021/acsnano.8b07104.

Persistent Link:
https://hdl.handle.net/11343/345826

The Effects of Hydrostatic Pressure on the Surface Plasmon Resonance of Gold Nanocrystals

Camino Martín-Sánchez[a], *José Antonio Barreda-Argüeso*[a], *Susanne Seibt*[b], *Paul Mulvaney*[*,b], *Fernando Rodríguez*[*,a]

[a] MALTA CONSOLIDER TEAM, DCITIMAC, Facultad de Ciencias, University of Cantabria, Santander, 39005, Spain.

[b] ARC Centre of Excellence in Exciton Science, School of Chemistry, University of Melbourne, Victoria, 3010, Australia.

KEYWORDS: gold nanoparticles; hydrostatic pressure; surface plasmon resonance; optical absorption; bulk modulus, refractive index.

ABSTRACT

The surface plasmon resonances of gold nanospheres and nanorods have been measured as a function of hydrostatic pressure up to 17 GPa in methanol-ethanol 4:1 solvent and up to 10 GPa in paraffin. Both the sphere resonance and the longitudinal rod resonance exhibit redshifts while the transverse rod mode shows an extremely weak redshift or blueshift depending on the nanorod aspect ratio. Solidification of the solvent around 11 GPa causes some aggregation of the particles, readily identified through broadening of the SP band and further redshifting. Loading and unloading cycles show only minimal hysteresis in the spectra if the pressure remains below 11 GPa. The surface plasmon shifts are the result of two competing effects. Compression of the conduction electrons in the metals increases the bulk plasma frequency, which causes a blueshift. However, the increase in the solvent density under hydrostatic load leads to an increase in the solvent refractive index, which in turn leads to a redshift. We find that after accounting for the solvent contribution, we can spectroscopically determine the bulk modulus of the gold nanoparticles with a precision of 10%. The value obtained of K_0 = 190 GPa is significantly higher than the value for bulk gold (167 GPa). Furthermore, we show that pressure-induced solidification causes a significant broadening and anomalous shift of the surface plasmon band that we attribute to aggregation and nanorod deformation.

Nanoscale materials exhibit size-dependent optical, magnetic, electronic, and catalytic properties, and are very promising candidates for applications ranging from biomedicine to electronic displays.[1-3] However, measurement of the mechanical properties of nanocrystals has remained a major challenge because of the difficulty of applying well-defined loading forces to the materials and the problems of measuring deformations accurately. Some theoretical models predict that nanoscale materials possess superior mechanical strength because of the lack of large-scale crystal defects such as grain boundaries and dislocations. Conversely, other dynamic models predict instability because the high surface energy of nanocrystals leads to enhanced surface diffusion of ions, lower melting points, increased solubility and stress induced shape changes. To resolve these questions, new experimental methods are needed to study the mechanical properties of nanoscale materials.

Particularly attractive are spectroscopic approaches, which exploit the optical transparency of nanocrystals. For example, Hartland and colleagues have shown that pulsed laser excitation of a gold rod or sphere excites fundamental breathing and stretching modes in the crystals and the frequency of these vibrations (GHz regime) can be used to extract the Young's modulus.[4]

Although hydrostatic pressure measurements have been carried out on various semiconductor nanocrystals,[5,6] previous measurements on metallic nanoparticles have been carried out only under quasi-hydrostatic regimes [7] or in non-hydrostatic regimes [8,9] where the nanoparticles were embedded in a matrix of ice or phosphate glass, respectively. Here we present the first spectroscopic measurements on metal nanoparticles under hydrostatic loading to study the changes in the surface plasmon resonance (SPR) of small gold spheres and nanorods. To preserve hydrostatic conditions under high pressure, we prepared suitable solutions of gold nanorods (GNR) using different methanol-ethanol mixtures (MeOH-EtOH) – the 4:1 mixture is

hydrostatic up to 11 GPa. We also explored paraffin as a solvent because it is easier to stabilize nanocrystals in non-polar media and we also utilized a MeOH-EtOH (1:4) mixture as a solvent, which solidifies at 4 GPa at room temperature. Optical absorption measurements up to 15 GPa enabled us to explore how pressure affected the solvent refractive index, conduction electron density in the metal[10] and the shape and size of the nanoparticles.[11,12] We will demonstrate that we can use these spectral shifts to deduce the mechanical stiffness of the crystals.

RESULTS/DISCUSSION

Scheme 1 shows the optical set-up used to record the absorption spectra of the nanocrystals as a function of hydrostatic load.

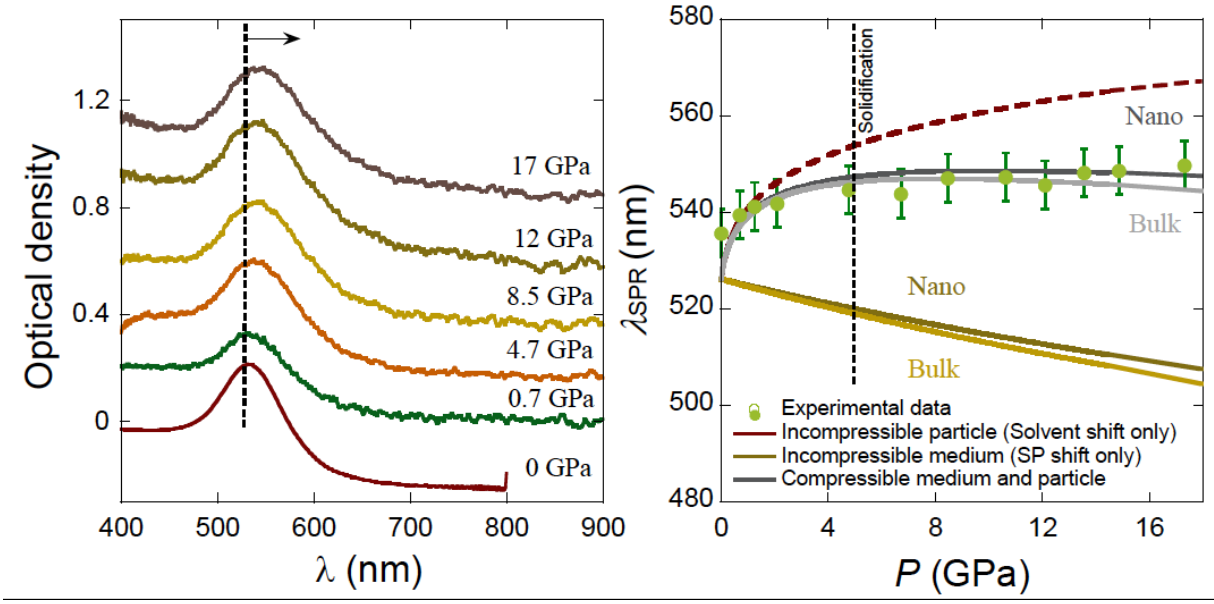

Figure 1: (Left) Spectra of 20 nm gold nanospheres coated with octadecyl amine in paraffin as a function of pressure. The SP resonance at 530 nm redshifts with increasing load and blueshifts reversibly with decreasing pressure. (Right) Plot of the peak wavelength vs pressure. Green data points: Experimental data. Dashed red line: Numerical fit assuming no change to the bulk plasma frequency (incompressible particle). Solid Brown Lines: Fit for a gold nanoparticle or bulk gold material assuming an incompressible solvent. Black and Grey lines: Fits using a value of K_0 =190 GPa (black) and the bulk metallic gold modulus (grey) of K_0 =167 GPa and assuming K_0'=

6 in both cases.[14] See Figure S5 for calculation details. Error bars correspond to the standard deviation derived from the fit of the SPR band to a log-normal function.

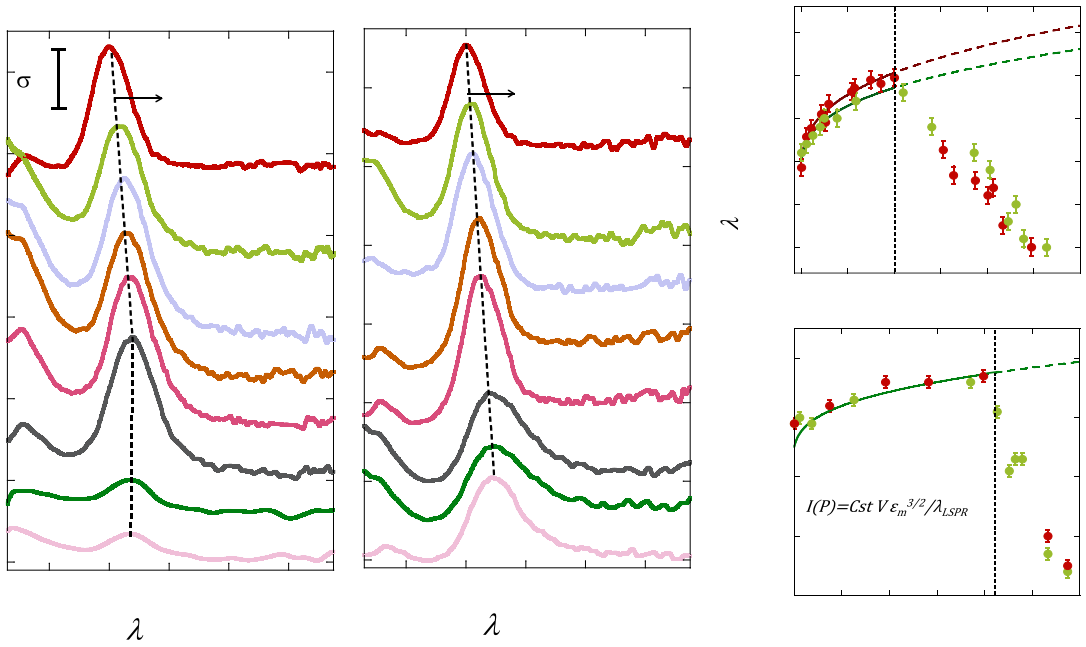

Figure 2: (Left) Spectra of 21.7 nm × 5.6 nm gold nanorods coated with PVP in 4:1 and (Middle) 1:4 MeOH-EtOH as a function of hydrostatic pressure. The SPR peak wavelength at 835 nm redshifts strongly with increasing load and blueshifts during unloading (see Figure 3, and Figures S3 and S4 in the SI). (Right) Plot of the optical density at the LSPR peak maximum vs pressure. Solid line: calculated extinction cross section from Mie-Gans theory for the two GNR (AR = 3.7) solutions. Dashed line: calculated absorption in the solidified solutions using ε_m values of the liquid solution. Note the abrupt deviation of the experimental points at the solidification pressures: 8 and 4 GPa, respectively.

The variations in the absorption spectra of GNS in paraffin (Figure 1) and GNR in MeOH-EtOH (Figures 2-3) with pressure demonstrate that gold nanoparticle solutions are very sensitive to pressure. A clear, pressure-induced redshift of the surface plasmon resonance is observed for all GNS and GNR solutions. The magnitude of the redshift increases for GNRs with larger aspect ratios (AR), with the longitudinal surface plasmon resonance (LSPR) shifting in the 0-10 GPa

range by about 3% of the SPR wavelength for GNS and up to 9% for GNR solutions (AR = 4.9). Indeed, the pressure-induced redshift of the AR = 4.9 GNR solution is 69 nm/GPa (0.12 eV/GPa) in the 0-0.5 nm range, which is the largest pressure shift recorded to date. Smaller shifts are also observed for the transverse resonance with pressure (Figures 2-3) and there is an increase in the optical density with increasing pressure.

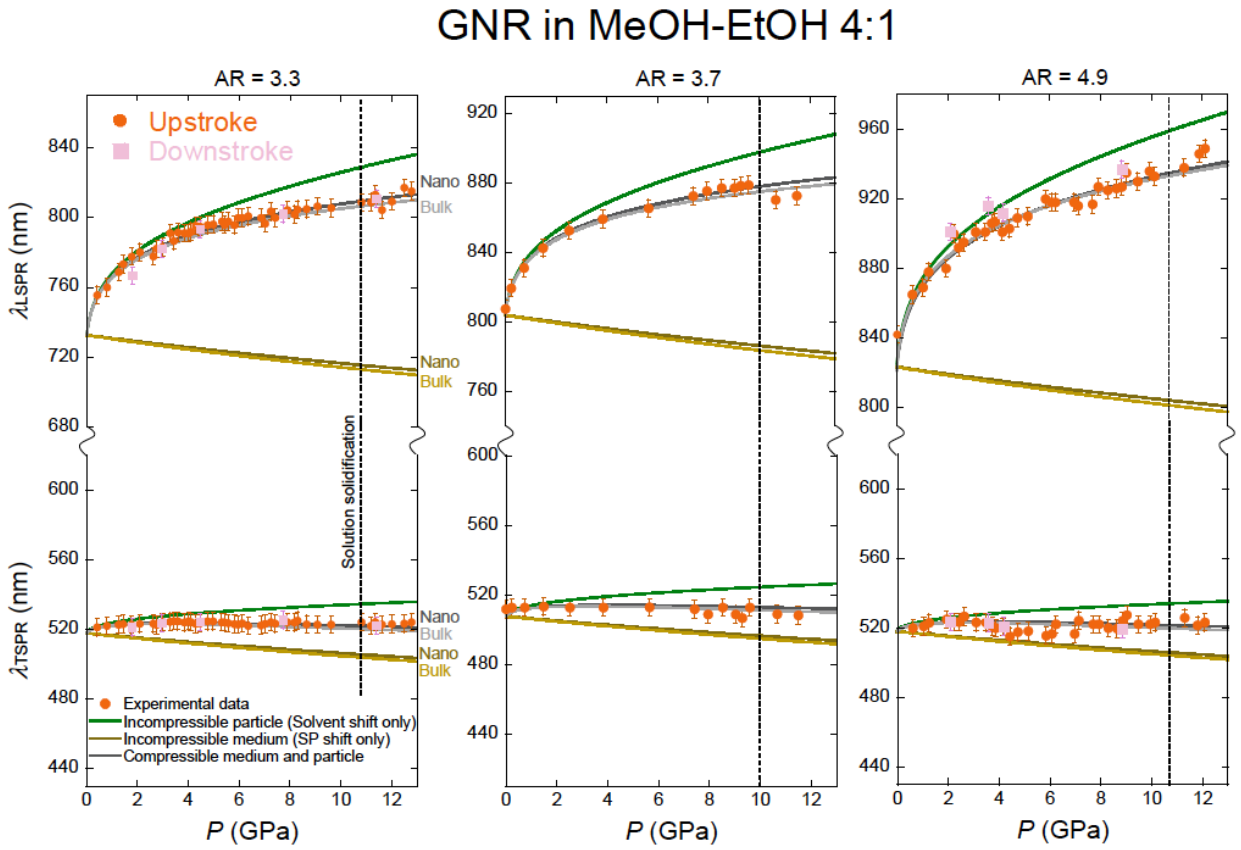

Figure 3: Pressure dependence of the LSPR and TSPR peaks for 42.2 nm × 12.8 nm (AR = 3.3), 21.7 nm × 5.6 nm (AR = 3.7) and 28.5 nm × 5.8 nm (AR = 4.9) GNR coated with PVP in 4:1 and 1:4 MeOH-EtOH as a function of pressure (left and right plots, respectively). Plots include experimental and calculated values of $\lambda_{LSPR}(P)$ and $\lambda_{TSPR}(P)$ using the Mie-Gans model. This model accounts for the SPR behavior in the hydrostatic regime but there are substantial deviations above the solidification pressure. Filled circles correspond to experimental data, and lines represent the calculated LSPR and TSPR wavelengths for: (brown line) incompressible medium; (green line) incompressible particle and for compressible solvent and particle (grey line) using both the bulk modulus of metallic gold and the fitted bulk modulus (Nano) to the

experimental data. Calculation details are given in the discussion section and Figures S4 and S5 in the SI.

We interpret the results in terms of the Mie-Gans model.[13] For small particles satisfying the Rayleigh conditions, the extinction of light is primarily due to dipolar excitations and the following expressions should be valid [17]

$$\sigma_{ext} = \sigma_{abs} + \sigma_{sca} = k\,\mathrm{Im}(\alpha) \qquad \text{with} \quad \sigma_{sca} = \frac{k^4}{6\pi}|\alpha|^2 \qquad (1)$$

Here σ_{ext} is the extinction cross-section of the nanocrystal solution in terms of the optical polarization, α, and the wavevector of the incident light, $k = 2\pi n/\lambda$. There are two contributions due to photon absorption and photon scattering by the nanocrystal. The polarizability of a small particle along the principal directions of the ellipsoid is given by[1, 2]

$$\alpha_{x,y,z} = \frac{4\pi}{3} abc\, \frac{\varepsilon_{Au} - \varepsilon_m}{\varepsilon_m + L_{x,y,z}(\varepsilon_{Au} - \varepsilon_m)} \qquad (2)$$

Here *a*, *b* and *c* are the radii in the case of a sphere (*r* = *a* = *b* = *c*) or the semi-axes in the case of a rod (*a* > *b* = *c*), ε_{Au} is the dielectric function of the particle[19] and $\varepsilon_m = n^2$ is the dielectric function of the non-absorbing medium, which also yields a refractive index, *n*. $L_{x,y,z}$ is the depolarization or shape factor, defined for ellipsoids as[1, 2]

$$L_x = \frac{1 - e^2}{e^2}\left[-1 + \frac{1}{2e}\ln\left(\frac{1+e}{1-e}\right)\right] \qquad (3)$$

$$L_y = \frac{1 - L_x}{2} \qquad (4)$$

where $e^2 = 1 - (b/a)^2$ is the ellipticity of the particle (*e* = 0 and *L* = 1/3 for a sphere). For spherically capped cylinders, the value of L can be treated as a fitting parameter or determined numerically.[12] For gold, the Drude model accurately predicts the dielectric response and we have

$$\varepsilon_{Au}(\omega) = \varepsilon_{\infty} - \frac{\omega_p^2}{\omega(\omega + i\gamma)} \quad (5)$$

Here ε_{∞} is the high frequency limit and incorporates interband and higher energy core transitions in the metal, $g$is the damping frequency and $\omega_p^2 = \frac{Ne^2}{m\varepsilon_0}$ defines the bulk plasma frequency of the metal.[17-19] From Equation 2, the surface plasmon resonance condition is fulfilled when:

$$(1 - L)\varepsilon_m + L\varepsilon_{Au}(\omega) = 0 \quad (6)$$

Any change to the parameters L, ε_{Au} or ε_m in Equation 6 will alter the surface plasmon peak wavelength.

Hydrostatic pressure can alter the polarizability and hence the absorption spectrum through at least 4 distinct mechanisms. Firstly, the pressure can induce changes in *a*, *b*, and *c*. Because gold has a cubic (BCC) crystal structure the compression will be isotropic provided that the pressure transmitting medium is hydrostatic (fixed GNR aspect ratio). Hence, compression will slightly decrease the extinction coefficient, but this effect is not investigated further. Because there are small changes to the cell thickness during loading, the resultant changes in absorption coefficient are difficult to quantify. Secondly, if the strains along the various axes differ (non-hydrostatic conditions), then there will be a change in the shape factor L, which will cause the SPR to shift to higher or lower wavelengths. Thirdly, compression of the solvent will increase its density, leading to an increase in the solvent dielectric function, ε_m. Finally, the particle compression will cause an increase in the conduction electron density *N*. This increases the bulk plasma frequency, ω_p, and hence leads to a blueshift in the SPR wavelength.

The bulk modulus K, of a material with volume V, is defined in terms of the isothermal compressibility B as

$$\frac{1}{K} = B = \frac{1}{V}\left(\frac{\partial V}{\partial P}\right)_T \quad (7)$$

The bulk plasma frequency depends on the particle volume as follows:

$$\frac{\omega_p^2(P)}{\omega_p^2(0)} = \frac{V_0}{V(P)} \quad (8)$$

or, in terms of the plasma wavelength: $\lambda_p(P)/\lambda_p(0) = \sqrt{V(P)/V_0}$. We can directly correlate the spectral shifts in the SP mode to relative changes in the volume of the particle at each pressure. Normally the value of K is obtained by fitting the (P,V) data to an Equation of State (EOS), that in the case of a first-order Murnaghan EOS is given by

$$P = \frac{K_0}{K_0'}\left[\left(\frac{V_0}{V}\right)^{K_0'} - 1\right] \quad (9)$$

Here $K = K_0 + K_0'P$ and $K_0' = \left(\frac{\partial K}{\partial P}\right)_{P=0}$. Hence the analysis consists of measuring the spectra of the gold nanocrystals over a range of hydrostatic pressures and using the spectral shift to calculate the change in particle volume at each pressure (see Figure S1 in the SI). The model considers the aspect ratio distribution of the solution, the end-cap geometry of the particles and the presence of the surfactant molecules.[22] The complete plot of P vs V is then fit to Equation 9 to yield the bulk modulus keeping the first derivative fixed at $K_0' = 6$.[10,14]

The above analysis holds provided that the particles do not change shape under a hydrostatic load. Such changes would result in plastic deformations and would be irreversible. We see little hysteresis in the $P(V)$ data and hence conclude that shape changes are not significant. We also saw no significant change in particle shape by TEM after experiments. The above analysis also holds only if the solvent refractive index does not change. Rearranging Equation 6 yields:

$$\lambda_{LSPR}(P) = \lambda_p(0)\sqrt{\frac{V}{V_0}}\sqrt{\varepsilon(0) + \frac{1-L}{L}\varepsilon_m(P)} \quad (10)$$

To model the changes in the solvent with increasing pressure, the dielectric function, $\varepsilon_m(P)$, is fitted empirically to a Lorentz-Lorentz relation:

$$\varepsilon_m(P) = n^2 = \frac{1+2u}{1-u} \quad (11)$$

where $u = \frac{4\pi}{3}\frac{N_A}{V_0}\left(\frac{V_0}{V}\right)\alpha_P$. Here N_A is Avogadro's number, V_0 the zero-pressure molar volume, α_P, is the molecular polarizability at *P*, and can be described empirically by the equation $\alpha_P = \alpha_0\left(\frac{V_0}{V}\right)^{\varphi}$ with φ = -0.157 for MeOH-EtOH (4:1).[15] Using a Tait EOS for the solvent:[20]

$$\frac{V}{V_0} = 1 - \frac{1}{(K_0'+1)}ln\left[\frac{(K_0'+1)P}{K_0} + 1\right] \quad (12)$$

we obtain a precise description of the refractive index (and hence dielectric function) of the solvent as a function of pressure by fitting the measured values to the equation:

$$\varepsilon_m = \frac{1 + 2C_0\left(\frac{V_0}{V}\right)^{1+\varphi}}{1 - C_0\left(\frac{V_0}{V}\right)^{1+\varphi}} \quad (13)$$

where $C_0 = \frac{4\pi}{3}\frac{N_A}{V_0}\alpha_0$ and φ are determined by fitting the experimental refractive index data as a function of pressure to Equation 13, and the *V*(*P*) data to Equation 12 for the corresponding solvent. From the available refractive index data as a function of pressure and *V*(*P*) data for liquid paraffin in the 0-1.9 GPa range[16] and liquid MeOH-EtOH (4:1) in the 0-11 GPa range,[12] the obtained fitting parameters are: C_0 = 0.2831; K_0 = 1.46 GPa; K_0' = 13; and φ = -0.016 for paraffin (Figure S5 in the SI), and C_0 = 0.2109; K_0 = 0.77 GPa; K_0' = 9.9; and φ = -0.157 for MeOH-EtOH.

The data in Figures 1-3 were fit to Equations 11-13 and the fits are shown using the gold bulk modulus (K_0 = 167 GPa),[14] and the fitted one, labelled "Nano" (K_0 = 190 GPa), with a fixed value of K_0'= 6 in both cases. In the simplest case, the observed surface plasmon wavelength is plotted as a function of the applied pressure and the values of K_0 and K_0' are obtained. Better fits were obtained when the plasma wavelength or high frequency dielectric constant were also included as fitting parameters. For both spheres and rods, the refractive index induced redshift is higher than the blueshift due to the electron gas compression. However, we can subtract the solvent effect and use this to find a value of K_0. Interestingly, the obtained value of 190 GPa is significantly higher than the bulk modulus for gold metal. X-ray diffraction experiments on compacted GNS samples under non-hydrostatic conditions show that the GNS equation of state is well described by a bulk modulus of K_0 = 196 GPa,[6] supporting the present findings, which were obtained under hydrostatic conditions. As is shown in Figures 2 and 3, a bulk modulus about 10% larger than the modulus for bulk gold best describes the observed variations in the LSPR cross-sections as a function of pressure for all the GNR solutions. This result is predicated on the assumption that $\varepsilon(0)$ remains constant with pressure and provides experimental evidence for bulk modulus enhancement for GNRs, whose specific surface energy increases with pressure. Although the interband transitions may lead to a variation in $\varepsilon(0)$ with pressure, our conclusions are based on the shape of the LSPR(P) variation of GNR outside the wavelength region where the interband effects are important ($\lambda > 590$ nm). Furthermore, a variation in $\varepsilon(0)$ with pressure is not simultaneously consistent with the red-shift of the longitudinal modes and the small blue-shifts observed for the transverse surface plasmon polariton mode.

The depolarization factor L is smaller for the longitudinal mode than for the transverse mode of the GNR (see Equations 2-4, 10), which leads to a stronger sensitivity to refractive index changes, *i.e.* larger LSPR redshifts. For the LSPR mode, the refractive index induced redshift is larger than the blueshift due to plasmon compression. This contrasts with the small transversal surface plasmon resonance (TSPR) blueshift observed in Figure 3, where the effect of compression of the electron gas is more important than the solvent induced shift. Since the increase in solvent refractive index must lead to a TSPR redshift, the observed blueshift confirms that there is an increase in electron density and compression of the GNR.

Based on the bulk modulus of metallic gold, K_0 = 167 GPa,[14] the relative electron concentration ($N/N_0=V_0/V$) increases by about 6% at 10 GPa. The corresponding relative increase in the bulk plasma frequency is 3%, which is detectable by optical spectroscopy through the SPR shifts, provided that we know the contributions from the surrounding media. Interestingly, the gold EOS is known [10,14] (although only under non-hydrostatic conditions for GNS)[6], and the refractive index of the solvent as a function of pressure is known experimentally.[15,16] This knowledge allows us to simulate the variations of SPR and the total absorption cross section of the SPR, by fixing the pressure dependences of $N(P)$ and $\varepsilon_m(P)$. This is not the case for paraffin where the pressure-dependence of refraction index is known only over a narrow pressure range (0-1.9 GPa).[15]

The anomalous optical absorption at the LSPR peak observed in Figure 2 is noteworthy. The deviation of the experimental absorption intensity data, $I(P)$, from the calculated absorption from Mie-Gans theory,[13] which fairly describes the observed pressure-induced GNR solution absorption at the LSPR peak in liquid state, shows an abrupt decrease in $I(P)$ above the solution

solidification pressure. The higher the solidification pressure, the more abrupt the absorption decay. This effect is accompanied by an important broadening of the LSPR band.

CONCLUSIONS

In conclusion, we have measured the effects of hydrostatic loading on the surface plasmon resonances of gold nanospheres and nanorods. We have extracted the bulk modulus from the experiments and found it to be 190 GPa, about 15 % higher than the bulk modulus for gold metal. Other key points are:

1) GNR solutions in MeOH-EtOH (1:4) are well suited for obtaining absorption spectra in the hydrostatic (1-4 GPa) and non-hydrostatic (P > 4 GPa) regimes. Mie-Gans theory fairly accounts for the pressure-induced SPR shifts and variations of extinction cross-section in the hydrostatic regime. However, it is inadequate for describing the GNR spectral catastrophe observed under non-hydrostatic conditions (see Figure 2 and Figure S4 in the SI).

2) GNR solutions in MeOH-EtOH (4:1) provide a wider hydrostatic range (about 1-10 GPa) and thus a wider pressure range for describing spectral variations on the basis of the Mie-Gans theory in the hydrostatic regime. Nevertheless, non-hydrostatic effects (P > 10GPa) are stronger when solution solidification takes place at higher pressures.

3) GNS solutions exhibit smaller changes in the SPR with pressure due to the larger geometric shape factor, L = 1/3, which reduces the solvent influence. Mie-Gans theory does not account quantitatively for variations of the SPR and σ_{ext} with pressure for the spheres. We also found that poorer fits were obtained when we fitted the high-pressure spectral shifts to the EOS and refractive index data extrapolated from low-pressure measurements. Indeed, a better estimation of n(P) can be obtained by fitting the paraffin EOS, and hence n(P) to the experimental SPR data. This is an interesting application of plasmonics to refractive index sensing. It is noteworthy that

the spectral shifts in the GNR solutions provide a sensitive marker for the onset of non-hydrostatic effects.

4) Finally, we note that the pressure-induced redshift of the SPR in the low-pressure regime (< 0.5 GPa) is one of the largest measured ever: 69 nm/GPa (0.12 eV/GPa). Furthermore, we also observed that the nanocrystal solutions solidified at a different pressure to the pure solvent and that non-hydrostatic conditions result in irreversible changes to the GNR spectra. Pressure-induced solution solidification results in nanorod aggregation and/or shear and compressive deformations after solvent-solidification.

EXPERIMENTAL METHODS

Synthesis:

GNR solutions in MeOH-EtOH solvents were prepared using hydroquinone as the reductant.[22] After rod growth they were purified by centrifugation to remove CTAB and unreacted spectator ions. The GNRs with aspect ratios 3.3 or 5.7 were stabilized in MeOH-EtOH solutions using poly(vinylpyrrolidone), MW ~ 10,000 g/mol as surfactant. Gold nanospheres (GNS) in paraffin were prepared by phase transfer of a Turkevich gold sol from water into paraffin using octadecylamine as phase transfer agent. Electron microscopy images were obtained on a Tecnai FEI20 TEM instrument at 200kV (Figure 4). TEM reveals the GNRs to be spherically capped cylinders. The absorption spectra of the GNR solutions exhibit the characteristic intense LSPR and weak TSPR peaks, the wavelengths of which show a linear redshift with aspect ratio (Figure 4). Fits are shown using Mie-Gans theory (see Figures S1-S2 in the Supp. Info.).

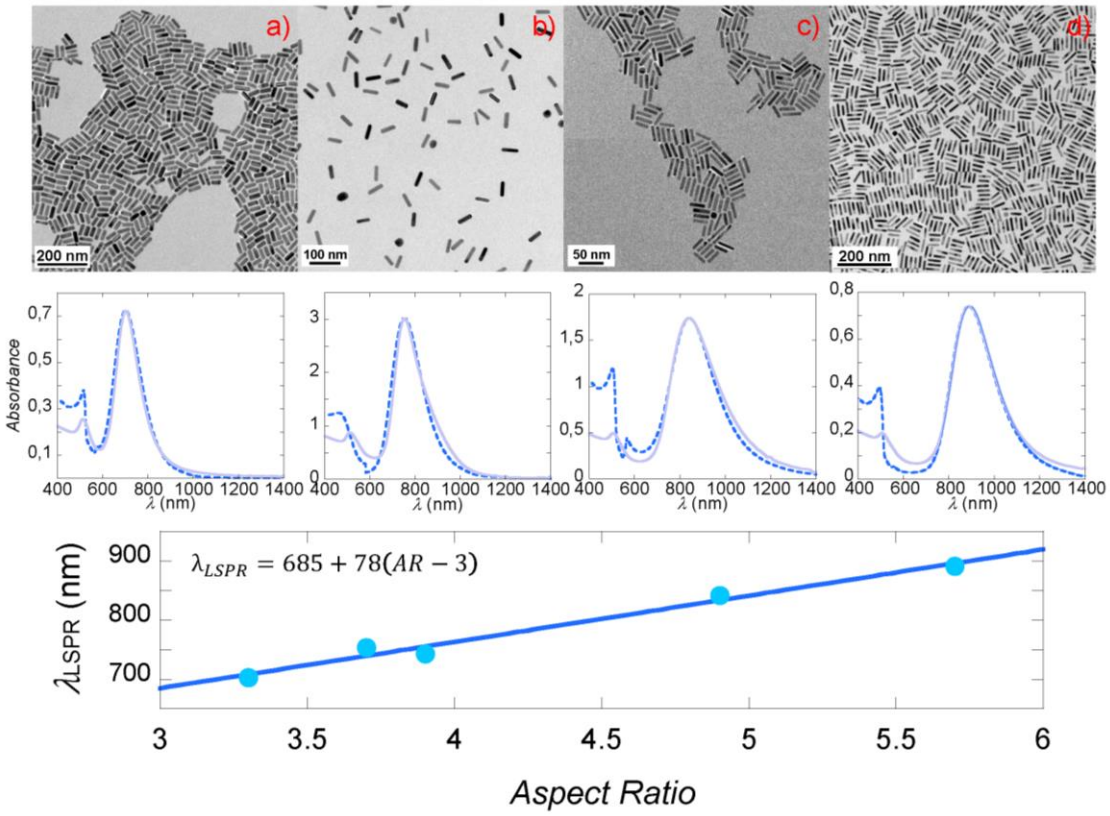

Figure 4: TEM images of the gold nanorods used in these experiments. High resolution images show the particles to be single crystals with the major growth direction being [1 0 0]. Particles resemble spherically capped cylinders. The aspect ratios, mean lengths and widths are: a) AR =3.3, $l(2a)$ = 42.2 nm, $d(2b)$ = 12.8 nm; b) AR = 3.7, l = 21.7 nm d = 5.6 nm c) AR = 4.9, l = 28.5 nm, d = 5.8 nm; d) AR = 5.7, l = 43.0 nm, d = 7.4 nm. Optical absorption spectra of the corresponding GNR solutions showing the variation of the LSPR peaks with the GNR aspect ratio, and the corresponding calculated one from Mie-Gans theory (see Figures S1-S2 in the SI).

A Cary 6000i spectrophotometer was used to collect the optical absorption spectra of GNR and GNS solutions in the 300-1700 nm range using either paraffin or MeOH-EtOH as references. Suitable silica-grade cuvettes with pathlengths of 1, 0.1, or 0.01 cm were employed depending on the GNR and GNS concentrations. The absorption spectra were obtained after sonication of solutions for 10 min. to ensure complete dispersion. Spectra were collected as a function of time

to check colloid stability. Both the shape and SPR peak wavelength were stable to within 5% over the time scales of the experiments.

Measurements:

High-pressure experiments were carried out in membrane and Böehler-Almax diamnod anvil cells (DACs). 200-μm-thick Inconel gaskets were preindented to 40-70 μm. 150-μm-diameter holes were perforated with a BETSA motorized electrical discharge machine and used as hydrostatic chambers. The DAC was loaded with suitable MeOH-EtOH GNR or paraffin GNS solutions and ruby microspheres (10-20 μm diameter) as pressure probes.[23] The solution itself acted as the pressure-transmitting medium. The hydrostaticity of the pressure transmitting media was probed through the ruby R-line broadening, the linewidth of which is known to slightly decrease with pressure in the hydrostatic range. However, it undergoes an abrupt broadening with increasing pressure in a solidified pressure-transmitting medium.[24] The alcohol based GNR solutions were loaded rapidly (a few seconds time scale) in order to minimize solvent evaporation. Depending on the loading procedure (loading time or cavity thickness), the spectra showed small deviations of the SPR (about 10-30 nm) that we attribute to adsorption of a small fraction of the GNRs onto the diamond culets.

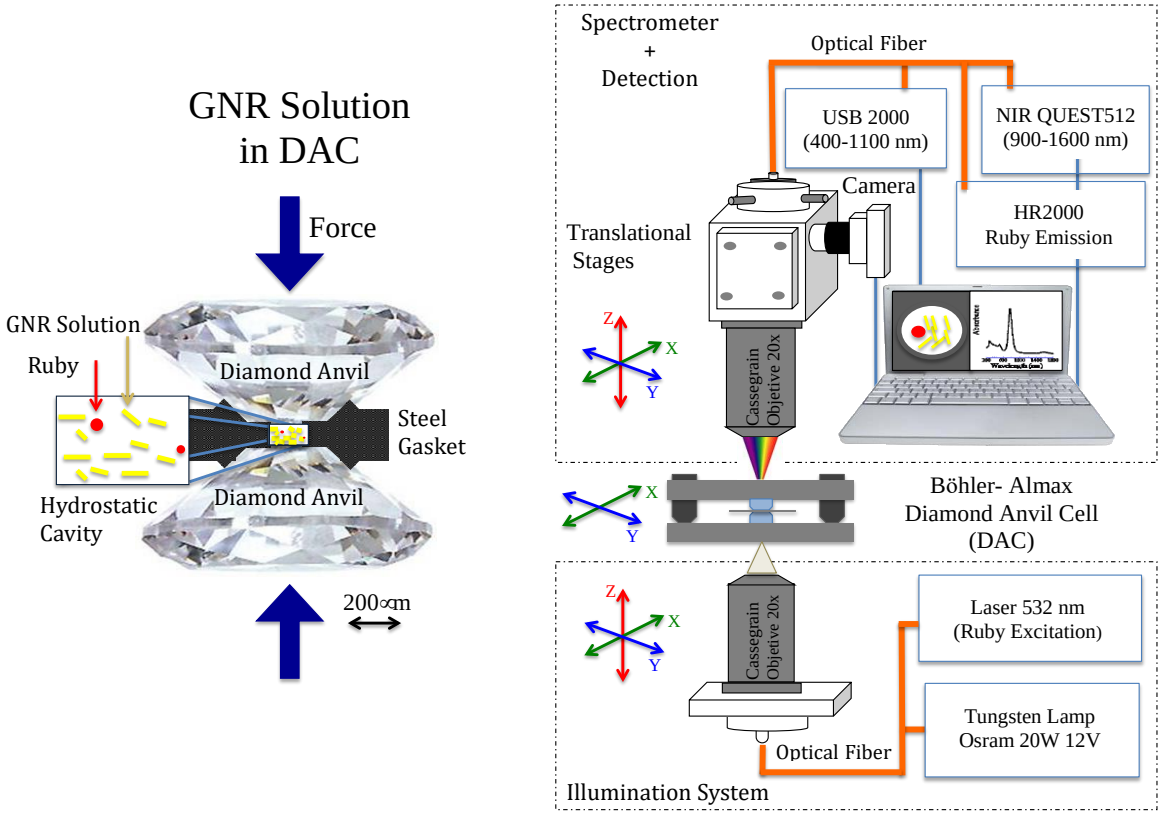

Scheme 1: High-Pressure optical spectroscopy. (Left) Diagram showing the set-up for the DAC. The volume of the cell is about 10 nL before it is loaded. (Right) Diagram showing the optical set-up to generate both the reference and sample beams using optic fibers for collection of absorption spectra.

Optical absorption spectra under high-pressure conditions were collected on a home-built fiber-optic based microscope, equipped with two Cassegrain 20× reflecting objectives mounted on two independent *x -y -z* translational stages for the microfocus beam, the objective lens and a third independent *x-y* translation stage for the DAC holder. Optical absorption data and images were obtained simultaneously with the same device.[25] Spectra in the UV-VIS and NIR were recorded with 2 spectrometers, an Ocean Optics USB 2000 and a NIRQUEST 512, employing Si- and InGaAs-CCD detectors, respectively. The I and I_o intensities were measured in two separate

experiments with the same DAC by loading it first with the nanoparticle solution (I), and then with the corresponding solvent (I_o), covering the same pressure range. Three independent experiments were performed for each of the three investigated solutions: GNR in MeOH-EtOH (1:4 and 4:1) and GNS in paraffin. The hydrostatic pressure range and liquid-solid pressure transition of GNR and GNS solutions were determined from the pressure dependence of the full width at half maximum (FWHM) of the Ruby R-lines (see Figure S3 in the SI).[23,24]

ASSOCIATED CONTENT

Supporting Information.

Supporting Information (SI) contains detailed information on the following items. 1) Calculated spectra from Mie-Gans model: aspect-ratio distribution and plasmon frequency. 2) Variation of the LSPR and TSPR wavelength with the aspect ratio. 3) Hydrostaticity of the GNR solutions as pressure transmitting media: Liquid-Solid transition pressure. 4) Non-hydrostatic effects on the SPR shifts. 5) Equations describing the EOS and refractive index of paraffin as a function of pressure. Supporting Information Available online.

AUTHOR INFORMATION

Corresponding Authors

* Fernando Rodríguez. E-mail address: rodriguf@unican.es

* Paul Mulvaney. E-mail address: mulvaney@unimelb.edu.au

Author Contributions

The manuscript was written through contributions from all authors. All authors have approved the final version of the manuscript.

Funding Sources

MAT2015-69508-P (MINECO/FEDER)

MAT2015-71070-REDC (MALTA TEAM /MINECO)

ACKNOWLEDGEMENTS

Financial support from Projects MAT2015-69508-P (MINECO/FEDER) and MAT2015-71070-REDC (MALTA TEAM /MINECO) is acknowledged. Fruitful discussions with L. M. Liz-Marzán are acknowledged. PM and SS acknowledge support from the Australian Research Council through grant CE170100026.

REFERENCES.

(1) El-Sayed, M. A. Small Is Different: Shape-, Size-, and Composition-Dependent Properties of Some Colloidal Semiconductor Nanocrystals. *Acc. Chem. Res.* **2004**, 37, 326-333.

(2) Pérez-Juste, J.; Pastoriza-Santos, I.; Liz-Marzán, J.M.; Mulvaney, P. Gold Nanorods: Synthesis, Characterization and Applications. *Coord. Chem. Rev.* 2005, *249*, 1870-1901.

(3) Nie, S.; Xing, Y.; Kim, G. J.; Simons, J. W. Nanotechnology Applications in Cancer. *Annu. Rev. Biomed. Eng.* **2007**, *9*, 257-288.

(4) Hartland, G. V.; Hu, M.; Wilson, O.; Mulvaney, P.; Sader, J. E. Coherent Excitation of Vibrational Modes in Gold Nanorods. *J. Phys. Chem. B* **2002**, *106*, 743-747.

(5) Tolbert, S.H.; Alivisatos, A.P. Size Dependence of a First Order Solid-Solid Phase Transition: The Wurtzite to Rock Salt Transformation in CdSe Nanocrystals. *Science* **1994**, 265, 373-376.

(6) Grant, C.G.; Crowhurst, J.C.; Hamel, S.; Williamson, A.J. Zaitseva, N, Anomalous Photoluminescence in CdSe Quantum-Dot Solids at High Pressure Due to Nonuniform Stress. *Small* **2008,** 4, 788-794.

(7) Gu, Wendy X.; Hanson, Lindsey A.; Eisler, Carissa N.; Koc, Matthew A:; Alivisatos, A. Paul.; Psudoelasticity at Large Strains in Au Nanocrystals. *Phys. Rev. Lett.* **2018**, 121, 056102.

(8) Bao, Y.; Zhao, B.; Tang, X.; Hou, D.; Cao, J.; Tang, S.; Liu, J.; Wang, F.; Cui, T.; Tuning Surface Plasmon Resonance by the Plastic Deformation of Au Nanoparticles within a Diamond Anvil Cell. *Appl. Phys. Lett.* **2015**, 107, 201909.

(9) Christofilos, D.; Assimopoulos, S.; Del Fatti, N.; Voisin, C.; Vallèe, F.; Kourouklis. G. A.; Ves, S.; High-pressure Study of the Surface Plasmon Resonance in Ag Nanopartilces. *High Pressure Res.* **2003**, 23, 23-27.

(10) Hong, X.; Duffy, T. S.; Em, L.; Weidner, D. F. *J.* Pressure-Induced Stiffness of Au Nanoparticles to 71 GPa Under Quasi-Hydrostatic Loading. *Phys.: Condens. Matter* **2015**, *27*, 485303.

(11) Link, S.; El-Sayed, M.A. Spectral Properties and Relaxation Dynamics of Surface Plasmon Electronic Oscillations in Gold and Silver Nanodots and Nanorods. *J. Phys. Chem. B* **1999**, 103, 8410-8426.

(12) Prescott, S.W.; Mulvaney, P. Gold Nanorod Extinction Spectra. *J. Appl. Phys.* **2006**, *99*, 123504.

(13) Gans, R.; Über die Form Ultramikroskopischer Goldteilchen. *Ann.Phys.* **1912**, *37*, 881-900.

(14) Heinz, D. L.; Jeanloz, R. The Equation of State of the Gold Calibration Standard. *J. Appl. Phys.* **1984**, *55*, 885.

(15) Eggert, J. H.; Xu, L. W.; Che, R. Z.; Chen, L. C.; Wang, J. F. High Pressure Refractive Index Measurements of 4:1 Methanol:Ethanol. *J. Appl. Phys.* **1992**, *72*, 2453.

(16) Poulter, T. C.; Ritchey, C.; Benz, C. A. The Effect of Pressure on the Refractive Index of Paraffin Oil and Glycerine. *Phys. Rev.* **1932**, *41*, 366-367.

(17) Bohren, C. F.; Huffman, D. R. *Absorption and Scattering of Light by Small Particles*; John Wiley & Sons. Inc.: New York, 1998.

(18) Johnson, P. B.; Christy, R. W. Optical Constants of the Noble Metals. *Phys. Rev.* **1972**, *6*, 4370-4379.

(19) Olmon, R. L.; Slovick, B.; Johnson, T. W.; Shelton, D.; Oh, S. H.; Boreman, G. D.; Raschke, M. B. Optical Dielectric Function of Gold. *Phys. Rev. B* **2012**, *86*, 235147.

(20) Tait, P. G. Report on Some of the Physical Properties of Fresh Water and Sea Water, Rept. Sci. Results Voy. H.M.S. Challenger. *Phys. Chem.* **1888**, *2*, 1.

(21) Pecharromán, C.; Pérez-Juste, J.; Mata-Osoro, G.; Liz-Marzán, L. M.; Mulvaney, P. Redshift of Surface Plasmon Modes of Small Gold Rods Due to their Atomic Roughness and End-Cap Geometry. *Phys. Rev. B.* **2008**, 77, 035418.

(22) Vigderman, L.; Zubarev, E.R. High-Yield Synthesis of Gold Nanorods with Longitudinal SPR Peak Greater than 1200 nm Using Hydroquinone as a Reducing Agent. *Chem. Mater.* **2013**, 25, 1450-1457.

(23) Syassen, K. Ruby Under Pressure. *High Pressure Res.* **2008**, *28*, 75-126.

(24) Klotz, S.; Chervin, J. C.; Munsch, P.; Le Marchand, G. Hydrostatic Limits of 11 Pressure Transmitting Media. *J. Phys. D: Appl. Phys.* **2009**, *42*, 075413.

(25) Barreda-Argüeso, J. A.; Rodríguez, F. Patent No. PCT/ES2014/000049.

BRIEFS.

The surface plasmon resonances of gold nanosphere and nanorod solutions have been measured as a function of hydrostatic pressure up to 17GPa. Both the sphere resonance and the longitudinal rod resonance exhibit redshifts while the transverse rod mode shows an extremely weak red-shift or blueshift depending on the nanorod aspect ratio. These shifts are the result of two competing effects: compression of the conduction electrons in the metals increases the bulk plasma frequency (blueshift) and increase of the refractive index of surrounding media (redshift). Pressure-induced solidification of the solvent causes some aggregation and deformation of the particles.

TOC